THE NATURAL CONFUSION LIMIT IN ULTRADEEP OPTICAL–IR AND RADIO SURVEYS

Rogier A. Windhorst[1], Seth H. Cohen, Nimish P. Hathi, Rolf A. Jansen, Stephen C. Odewahn

Department of Physics and Astronomy, Arizona State University, Tempe, AZ 85287-1504

{Rogier.Windhorst, Seth.Cohen, Nimish.Hathi, Rolf.Jansen, Stephen.Odewahn}@asu.edu

Simon P. Driver

Research School of Astronomy and Astrophysics, Australian National University, Cotter Road, Weston Creek, Canberra, ACT 2600, Australia

spd@mso.anu.edu.au

Daisuke Kawata, Brad K. Gibson

Centre for Astrophysics & Supercomputing, Swinburne University, Mail 31, P.O. Box 218, Hawthorn, Victoria, 3122, Australia

dkawata@astro.swin.edu.au, bgibson@astro.swin.edu.au

Jonathan P. Gardner

Goddard Space Flight Center, Code 681, Greenbelt, MD 20771

Jonathan.P.Gardner@nasa.gov

and

Andrew M. Hopkins

University of Pittsburgh, Department of Physics and Astronomy 3941 O'Hara Street, Pittsburgh, PA 15260

ahopkins@phyast.pitt.edu

---

[1]Interdisciplinary Scientist for the James Webb Space Telescope (JWST)

1. ABSTRACT

In this paper, we discuss the effects from the natural confusion limit on ultradeep optical-IR and radio surveys, using the newly released data from the Hubble Space Telescope (HST) Ultra Deep Field (UDF). While the *instrumental* confusion limit sets in when fewer than a certain number of instrumental beams — or Full Widths at Half Maximum (FWHM) of the instrumental Point Spread Function (PSF) — are available per detected object, the *natural* confusion limit sets in when fewer than a certain number of typical source half-light radii (r_{hl} or effective radii r_e) are available per detected object.

We estimate the natural confusion limit from the observed half-light radius (r_e) vs. total magnitude relation for the entire galaxy population from the RC3 level to the UDF limit ($A_B \lesssim$29-30 mag). We extend this relationship with ΛCDM cosmological simulations at flux levels J_{AB} (1.35 micron)$\simeq$29–34 mag, *i.e.*, beyond where they can be measured with the best HST UDF data available today. Together with model extrapolations of the faint galaxy counts at AB$\simeq$29–34 mag, we use the observed A_B -mag vs. r_e relation for $A_B \lesssim 29$ mag to estimate the natural confusion limit in the near-IR for the 6.5 meter James Webb Space Telescope (JWST) — planned for launch to an L2 orbit in 2011 — and at 1.4 GHz frequencies for the Square Kilometer Array (SKA). Both instruments will have resolutions $\lesssim 0\farcs1$ FWHM and will reach nanoJansky sensitivities (A_B =31–32 mag).

We find for ultradeep surveys with $\simeq 0\farcs1$ FWHM resolution, the natural confusion limit becomes *as important* as the traditional surface brightness (SB) limits. In particular, for resolutions of $\gtrsim 0\farcs08$ FWHM, at $J_{AB} \gtrsim 25$ mag ($B \gtrsim 27$ mag) both HST and the JWST may be more affected by natural confusion than by the traditional SB-limits. We suggest that this effect may already be visible in the deepest HST Hubble Deep Field (HDF) and UDF images, and could manifest itself in subtle biases in the "SExtractor" object-finding algorithm.

This does not mean that the deepest JWST samples will be fundamentally limited by natural confusion. Instead, due to their rapid hierarchical formation, the faint objects seen by JWST for $J_{AB} \gtrsim$28–30 mag will be largely point sources at $0\farcs08$ FWHM, which we begin to address here with ΛCDM cosmological simulations. In this case, only the very deepest JWST images will be limited by the *instrumental* confusion limit, which doesn't set in until around $J_{AB} \gtrsim 33.5$ mag. An important corollary of this finding is that in future ultradeep surveys, object-finding algorithms such as "SExtractor" will need to be more finely tuned to deal with object overlap.

Using these results for HST and JWST, we estimate the natural confusion limit for the SKA at GHz frequencies, assuming that the same population of faint irregular, peculiar and merging/star-forming objects that dominates the faint galaxy counts will likely dominate the radio source counts at nanoJansky levels. For such objects, their radio sizes are likely similar to, or at least not much larger than their optical–IR sizes. If so, the SKA will need to have better than 50–100 m.a.s. FWHM in order to not be limited by the instrumental

confusion limit at 100 nanoJy at 1.4 GHz. At levels of $S_{1.4}$ $\simeq$10 nanoJy, the SKA will reach similar object surface densities as the JWST at J_{AB} $\simeq$31–33 mag, and — like the JWST — not run into the natural confusion limit at $S_{1.4}$ $\simeq$10 nanoJy, *if* the slope of the nanoJy source counts remains flatter than $\gamma \lesssim 1.7$ (magnitude slope flatter than $\alpha \lesssim 0.28$), and if the ratio of radio to optical–near-IR sizes remains close to unity at nanoJy levels.

Keywords: galaxies: high-redshift — galaxies: surveys — galaxies: dwarfs — instruments: James Webb Space Telescope — instruments: Square Kilometer Array

2. INTRODUCTION

In the last few decades, very significant efforts have been made on deep surveys of the sky, ranging from radio to infra-red to optical and X-ray wavelengths. In the optical–near-IR, for instance, the "faint blue galaxy" (FBG) population that dominates the faint galaxy counts (Kron 1980; Koo & Tyson 1988; Ellis 1997) has been shown by HST to consist predominantly of late-type, irregular and peculiar galaxies (e.g., Driver et al. 1995, 1998; Glazebrook et al. 1995; Abraham et al. 1996; Odewahn et al. 1996) which vastly outnumber the expected surface densities seen in local surveys (Driver et al. 1998, Marzke et al. 1998). At radio wavelengths, the sub-milliJansky population similarly showed a significant excess in surface densities over those expected from brighter levels (Windhorst et al. 1985, 1993), which a number of groups have shown (Kron et al. 1985, Benn et al. 1992, Hammer et al. 1995, Windhorst et al. 1995; Hopkins et al. 1999) is likely due to a mixture of star-forming and merging galaxies in addition to increased AGN activity in faint early-type galaxies at intermediate to high redshifts. The tentative conclusion from these optical-IR and radio surveys has been that we see the effects of the gradual hierarchical formation of galaxies and their central engines over Hubble time.

Given the rapidly preceding technology of both telescope design, correlators, detectors and data processing techniques, telescopes are now under construction or in the design phase that will reach nano-Jansky sensitivities at both radio and optical–near-IR wavelengths, i.e. a full factor of 100–1000 times more sensitive than what can be achieved with current state of the art technology, *e.g.*, the Very Large Array (VLA), Very Long Baseline Interferometry (VLBI), the HST, and ground-based Adaptive Optics (AO). The IR telescope planned for the future is the 6.5 meter JWST (Mather & Stockman 2000, Stockman & Mather 2000), and at radio wavelengths the SKA is the planned next generation telescope (Hopkins et al. 2000; Ekers et al. 2000, Schilizzi et al. 2003).

A natural question to ask if whether the currently accomplished optical–near-IR and radio surveys show any evidence that the planned future surveys at nano-Jansky levels will run into the natural confusion limit. This is not only an important question to ask before significant investments are made in the final design and actual construction of these future telescopes, but also may provide insight as to whether we can extend future surveys to arbitrarily faint levels, or whether these surveys will run into fundamental limitations that will complicate their interpretation or perhaps make them impossible to carry out. Related to this, it may help answer the question whether the usual survey properties such as point-source (PS) sensitivity and surface-brightness (SB) sensitivity are the only limiting factors to the new surveys expected in the next decade, or whether other fundamental issues will ultimately limit these surveys. To our knowledge, these questions have not been posed in

this manner before, and so they are the main focus of the current paper.

To begin to answer these questions, we will in this paper first briefly review the classical instrumental confusion limit and the natural confusion limit (§3). Next, we summarize the available optical-red–near-IR counts of galaxies and their distribution over half-light radii, covering the widest possible range in flux. From this we estimate in §4 the natural confusion limit as expected for the 6.5 m JWST. In §5, we will similarly review the available radio source counts and their angular size distribution over the widest possible range in flux, and from this we will derive the natural confusion limit expected for the SKA.

3. THE TWO CONFUSION LIMITS CLARIFIED

3.1. The Classical or Instrumental Confusion Limit

The classical instrumental confusion limit occurs when the sensitivity of a telescope is so good that the faint source surface density results in significant source overlap — typically at the rate of a deep survey having fewer than 30–50 independent instrumental beams or FWHM's per detected object (Condon 1974), where the exact number of independent beams required for every detected source depends somewhat on the slope of the faint objects counts, following the P(D) analysis first introduced by Scheuer (1974). This effect hampers the construction of reliable and complete faint object samples and results in less reliable object catalogs (e.g., Windhorst et al. 1984; Bertin & Arnouts 1996).

3.2. The Natural Confusion Limit

The natural confusion limit occurs when the faint source population (with a median half-light radius r_e) is significantly resolved at the instrumental FWHM, *and* when their surface density is so high that one has fewer than a minimum number of "object beams" (with area $\pi \times r_e^2$) for each detected faint object. This is in essence based on the Rayleigh criterion, which requires two neighboring objects to be $\gtrsim$FWHM/2 apart to be detected as two separate objects.

The critical difference between the Instrumental Confusion Limit and the Natural Confusion Limit is thus only whether the instrumental beam FWHM is larger than the typical source size (measured through its median half-light radius r_e) or not. If FWHM$\gtrsim r_e$, then the survey will be limited by instrumental confusion *if it goes deep enough*, but if $r_e \gtrsim$FWHM it will be instead limited by natural confusion if it goes deep enough. We explain in this

paper here that there is a flux regime ($A_B \simeq$25–30 mag) where deep surveys will just touch on the natural confusion limit, but that in hierarchical formation models, surveys will be essentially only limited by instrumental confusion if they go deep enough.

4. Estimating the Natural Confusion Limit at optical–near-IR wavelengths

4.1. The Half-Light Radius vs. Total magnitude relation for the galaxy population

To compute the natural confusion limit for the JWST, we first need to summarize the half-light radius vs. magnitude relation for the entire galaxy population from the RC3 level to the HDF and UDF limits. In Fig. 2 we plot the total B-magnitude versus effective or half-light radius r_e for the entire galaxy population, as available today. Details are given in Cohen et al. (2002) for the RC3 and HST B-band parallel survey, in Liske et al. (2003) for the Millennium Galaxy Catalog (MGC) survey, and in Odewahn et al. (1996, 2002) for the HST HDF.

To this we added the A_B -mag vs. r_e data from the ACS parallels to the deep UDF NICMOS/NIC3 images, which are publicly available and which we similarly drizzled using the PyRAF multi-drizzle routines. We also used the multi-drizzled 150-orbit i-band UDF/ACS image as made available by STScI on March 9, 2004, which go about 1.5 mag fainter than the HDF and about 1.1 mag fainter than the the ACS parallels to the deep UDF NICMOS/NIC3 images.

4.2. How to deal with different restframe wavelengths sampled

It is important that the selected filter approximately approaches the sampled rest-frame galaxy Spectra Energy Distribution (SED). Since the local galaxy surveys (RC3 and MGC) are most uniformly done in the B-band and sample objects at redshifts $z \lesssim 0.2$, they typically sample the galaxy SED just long-ward of the 4000Å-break. The deep HST surveys such as the HDF and UDF cover $24 \lesssim A_B \lesssim 29$ mag and typically sample the galaxy population at $0.5 \lesssim z \lesssim 4$ with a peak in the redshift distribution N(z) typically at $1 \lesssim z \lesssim 2$, somewhat although not strongly depending on A_B -mag (Driver et al. 1998). Hence, the wavelength available closest to restframe $\lambda \gtrsim 4000$Å is the I, i, or z-band. We will therefore use the I-band or i-band images for the Deep Fields, since the UDF i-band is significantly deeper than the z-band image. We note that the wavelength dependence of the galaxy half-light radius r_e is small in any case (Cohen et al. 2003). Since the typical galaxy has a (B–I) color of 1.5 Vega-mag

($\sim$1.0 A_B -mag; Cohen et al. 2003), we will use the measured (B–I) vs. B-mag relation of Cohen et al. (2003) to plot the I or i-mags on the same scale as the Vega B-mags of the nearby surveys. This introduces subtle differences in the adopted flux-scale for the early-, mid- and late-type galaxy populations, but since the faint galaxy population is dominated by the blue late-type galaxies, these differences are smallest for the bulk of the faint galaxies, and as we will argue not detrimental to the broad arguments below. The natural confusion limit requires that we outline the r_e -values of the galaxy population between A_B =10 and A_B =35 mag (using ΛCDM cosmological simulations for $J_{AB} \gtrsim 29$ mag), so that small differences in the flux scale remaining after correcting for transformation from an I-mag to a B-mag scale will not significantly affect the overall picture. The same will be true for the JWST flux-scale, where we use the shortest wavelength expected to be used in bulk survey mode, the J-band or 1.35 μm filter. For field galaxies with $25 \lesssim A_B \lesssim 31$ mag, the median redshift is not exactly known, but following the models and arguments in Driver et al. (1998), the median redshift is probably in the range $1 \lesssim z_{med} \lesssim 3$, so that for the bulk of the objects the restframe wavelength sampled by the J-band is close to 4000Å or long-wards, so that comparison with the restframe B-band is appropriate. The SED of blue starforming galaxies with $1 \lesssim z_{med} \lesssim 3$ suggests that B_{Vega}–J_{AB} $\sim$2.0 mag, so that the JWST J_{AB} -fluxes can also be plotted in the same total flux vs. r_e diagram.

4.3. An Estimate of the Galaxy Counts to A_B =34 mag

To estimate the natural confusion limits, we also need an estimate the faint galaxy counts at J_{AB} (1.35μm) $\simeq$28–35 mag. For this, we use the galaxy count models of Gardner (1998) and Gardner & Satyapal (2000), which basically are a smooth extrapolation of the counts as measured to A_B $\simeq$30 mag with the HST HDF (WFPC2 and STIS), and include reasonable assumption about the LF and N(z) at fainter luminosities. Given the unknown role of faint dwarf galaxies, and perhaps new classes of objects not represented in these models, the model extrapolations to J_{AB} $\simeq$34 mag are at least uncertain in amplitude by 0.3 dex, which is of relatively little consequence in the argument that follows. In any case, at J_{AB} $\simeq$34 mag, the surface density of objects could be as high as 10–20$\times 10^6$ objects deg^{-2} (Fig. 1), or several detected objects per square arcsecond. Needless to say this implies that one would approach the natural confusion limit if the object sizes were still a good fraction of an arcsecond.

4.4. The Natural Confusion Limit for the James Webb Space Telescope

Here we address the natural confusion limit for the 6.5 meter James Webb Space Telescope (JWST), which is planned for launch to an L2 orbit in 2011 (Mather & Stockman 200; Im & Stockman 1999). The JWST telescope will have 18 hexagonal elements with a maximum diameter of 6.5 meter and an equivalent unobstructed circular aperture of 6.0 meter with the requirement that the geometric collecting area is no smaller than 25.0 sq. meter. JWST will have all gold reflective optics and cover the wavelength range 0.6–30μm. It will be diffraction limited at $\lambda \geq$2.0μm (or K-band with PSF FWHM$\gtrsim 0.084''$). Its primary near-IR camera, NIRCam, will have very high-QE low-noise detectors, and yield nanoJy sensitivities at 0.6-5.3μm (Rieke et al. 2002) in integrations of 10^5 sec. It will approximately reach J_{AB} $\simeq$31 mag at 10σ in 10-hrs, and it could reach J_{AB} $\simeq$33.5 mag in a dedicated 1000-hrs "super UDF-like" campaign.

We now estimate the natural confusion limit for JWST at 1.35 microns as following. From the observed slope of the galaxy counts (α $\simeq$0.3 for λ $\simeq$B$\rightarrow$K; Fig. 1 here, Maihara et al. 2001; Gardner et al. 2000) and the galaxy size distribution (Fig. 2–4), we predict the JWST *instrumental* confusion limit to occur at $J_{AB} \gtrsim 33.5$ mag, where the number of independent beams (with FWHM$\gtrsim 0''.084$) per detected object falls below 50 (*i.e.*, the classical confusion limit). The JWST *natural* confusion limit is assumed to occur when the galaxy density exceeds the level where there are fewer than 30–50$\times\pi$ r_e^2 "independent galaxy beams" for each detected object, which depends on the galaxy counts and size distribution for A_B $\gtrsim$29 mag. We estimate it from the above mentioned galaxy counts, and plot the resulting natural confusion limit as slanted pink lines in Fig. 3–4, which are plotted for 50, 10 and 1 beams per detected object. At the level of one detected object per available beam, the sky would be covered with half-light radii, and look like a CCD image of a globular cluster.

4.5. Results on the Natural Confusion Limit at optical–near-IR wavelengths

A rather unexpected scientific result of this study is that in ultradeep surveys, the natural confusion limit becomes *as* important in the definition of faint source samples as the traditional SB-limits. In particular, for resolutions of $\gtrsim 0''.08$ FWHM, it appears that for J_{AB} $\gtrsim$25 mag ($B \gtrsim 27$ mag) both HST and the JWST may be more affected by natural confusion than by the traditional SB-limits. We suggest that this may already be visible in the deepest HDF and UDF images, given how objects in Fig. 4 appear to stray away from the SB-limit lines (short-dashed) and appear to be closer to straddling the steeper slope of the natural confusion limit lines (long-dashed) for AB$\gtrsim$25 mag.

This does not mean that the deepest JWST samples will be fundamentally limited by natural confusion. Instead, we expect that for $J_{AB} \gtrsim 28$–30 mag, the faint objects seen by JWST will be largely point sources at 0.″08 FWHM, which we begin to address here with ΛCDM cosmological simulations using the models of Kawata & Gibson (2003a, 2003b) and Gibson et al. (2003).

The multi-resolution technique described in Kawata & Gibson (2003b) was used to resolve high-redshift galaxies in cosmological simulations, and hence predict their half-light radii, assuming that the light follows the mass. The mass and softening length of individual gas particles in our highest-resolution simulations are 3.4×10^4 $M_\odot$ and 0.075 kpc, respectively. The highest redshift of the simulated galaxies in Figure 4 is z=8.08. For some galaxies, we re-ran the simulations with different numerical resolutions, confirming within reason that the resolution of the simulations does not seriously affect the predicted half-light radii. We adopt a cosmology with Ω_0=0.3, Λ_0=0.7, $\Omega_{\rm b}$=0.019h^{-2}, h=0.7 and σ_8=0.9, and generate multi-resolution initial conditions using the public available software `GRAFIC2` (Bertschinger 2001). We analyzed the optical properties of simulated galaxies, using a similar population synthesis techniques as explained in Kawata (2001). Here, we use the simple stellar population of the public spectrum and chemical evolution code (Kodama & Arimoto 1997). We take the K-correction into the SED models, but do not apply any correction for dust absorption. Hence, the model luminosities that yield the fluxes plotted in Figure 4 are technically upper limits if dust plays a significant role. The effect of dust absorption on the observed r_e values is probably modest, as it is for nearby galaxies (de Jong 1996), indicating that the observed blue light is mostly in front of the dust slabs in inclined disk. Hence, we implicitly assume assume that dust does not change the estimated r_e for the galaxy population as a whole significantly, although the reader is cautioned that this could become a circular argument in surveys that explore the details of galaxy populations as a function of *e.g.*, inclination (Burstein et al. 1991). For the global trends that we seek to describe here, we ignore the effects from dust.

The first results of these ΛCDM cosmological simulations are shown as squares in Fig. 4. The good agreement between the black simulated galaxies and the observed colored points in the HDF for $B_J \lesssim 28$ mag gives us confidence that the few available simulations for $J_{AB} \gtrsim 26$ may yield accurate galaxy sizes. Also shown is the approximate size-range and expected flux-range for objects of globular cluster-type mass around the epoch of reionization (z≃7).

It is noteworthy that the expected object sizes for $A_B \gtrsim 28$ mag in Fig. 4 are mostly below the JWST diffraction limit (≃0.″08 FWHM), which we intend to confirm with further ΛCDM cosmological simulations. This is an issue of critical importance and its consequences are further discussed in §6. If most objects with $A_B \gtrsim 28$ mag are indeed unresolved by JWST,

then the deepest JWST images will be only limited by the instrumental confusion limit (as determined by JWST's instrumental FWHM$\simeq$0.″08), which doesn't set in until around J_{AB} $\gtrsim$ 33.5 mag. In that case, the hierarchical formation of galaxies together with the effects of the cosmological constant Λ at z$\lesssim$ 0.8 (Cohen et al. 2003) conspire to just keep the deepest JWST surveys away from the natural confusion limit in Fig. 4. These are important considerations for the precise definition of the FWHM and the exact PSF-shape of the JWST, which are currently being finalized.

5. Effects from Biases in the Object-Finder and Parameter-Estimating Algorithms

The natural confusion limits plotted in Fig. 3–4 are somewhat uncertain due to the unknown intrinsic object size distribution, and because it is unknown how far we can push overlapping galaxy images before we: (a) loose the ability to make complete and reliable faint object catalogs (e.g. Bertin & Arnouts 1996), and (b) measure accurate fluxes and structural properties (r_e etc.) of faint galaxies (e.g., Odewahn et al. 2002).

Simulations show that even with a perfect Gaussian PSF and in the absence of any neighbors, the fitted object parameters may be biased compared to what the input parameters were (Windhorst et al. 1984). This occurs, even in case of infinite S/N, because of the way algorithms fit the source parameters, and gets rapidly worse with lower S/N (with noise coming both from the sky and the detector). Adding neighbors whose wings can start overlapping makes the situation worse, and also complicates the way the sky-subtraction is being done. As a consequence, parameter determining algorithms may bias both the measured object sizes and fluxes, even if the S/N is large and worse when S/N the is small.

To address these issues, it may be that a new generation of object finding and parameter determining algorithms is needed that takes into account what is known about the PSF and the pix-to-pixel statistics of the image-noise, and makes best fits to each detected object while trying to optimally de-blend it from its neighbor. These algorithms may need to represent simple objects through analytically known light-profiles (Simard et al. 1999). In that sense, the SExtractor algorithm (Bertin & Arnouts 1996) commonly used on CCD images with faint objects may need to be updated to include the PSF and *simultaneous* object fitting techniques such as DOAPHOT and ALL-FRAME (Stetson 1989) do on deep crowded stellar CCD images. It is not clear that this can be straightforwardly done, but we hope to get the discussion for the need of such algorithms started through this paper. In a sequel paper, we will further address the limitations of existing object fitting algorithms on deep crowded CCD images with extended object.

To better model the natural confusion limit, we need also need to better model the expected intrinsic galaxy size distribution for the flux regime that is not yet sampled by the existing observations and that will not be sampled well until JWST comes along (*i.e.*, $J_{AB} \gtrsim 30$ mag). This requires both higher resolution ΛCDM cosmological simulations and better statistics of such simulations. This is a computationally expensive exercise, since for accurate determination or r_e , these simulations need to have high resolution and so can only cover relatively few objects in a limited volume. Larger samples of such high resolution simulations will help constrain the expected size distribution for $A_B \gtrsim 30$ mag, and result in a more accurate prediction for the JWST confusion limit for JWST. They may also help predict what kind of properties the new object finding and parameter determining algorithms need to have to optimally address the above issues.

6. The Natural Confusion Limit for the Square Kilometer Array

The Square Kilometer Array (SKA) radio interferometer is expected to become reality in the next decade (Hopkins et al. 2000, Ekers 2000, Schilizzi 2003). It will contain one square km of collecting area, and may exist of several thousand small (6 m) dishes placed in a geometrically increasing spiral pattern, and will likely have about 50% of the dishes in an inner core of 50 km maximum baseline that is heavily weighted towards high redshift H-I studies, and an outer core of $\lesssim 50\%$ of the dishes that are spread over maximum baselines of several 100 to several 1000 km. Its exact location and instrument and receiver, etc., design are as yet unknown, but will be determined in the next few years. The SKA will have will have unprecedented sensitivity and resolution at radio wavelengths in the regime of a few 100 MHz to many GHz. Its goals are to have 0.001–0.1″ FWHM, about 1° FOV, and to reach sensitivity at nanoJy levels (100 nJy at 5-sigma in 12-hrs, and a putative goal of 10 nJy in a "super-HDF-like" campaign of 1200 hrs).

Having set constraints to the JWST natural confusion limit, it is relatively straightforward to calculate it for the SKA at GHz frequencies. For this, we assume that the same population of faint irregular, peculiar and merging/star-forming objects that dominates the faint galaxy counts also likely dominate the radio source counts at nanoJansky levels (*e.g.*, Windhorst et al. 1985, 1993, 2001). For such starforming galaxies, their radio emission is purely caused by synchrotron emission from disks and star-forming regions (Condon 1989) — with only vanishingly small if any contribution from AGN. Hence, their sizes are likely similar to, or at least not much larger than their optical–IR sizes, which is corroborated by radio continuum– optical comparisons of such objects (Deeg et al. 1997). If so, like the JWST, the SKA will need to have better than 50–100 m.a.s. FWHM to resolve these objects

at high redshifts and not run into the instrumental natural confusion limit at 100 nanoJy at 1.4 GHz.

Critical for the natural confusion limit study is the faint radio source size distribution. In Fig. 5 we show the differential source counts and in Fig. 6 the median radio source size as a function of $S_{1.4}$ radio flux, with data from all available surveys as summarized in Windhorst et al. (1993, 2000) and updated with recent surveys. In general, the median radio source sizes decline steadily with radio flux over nearly 6 orders of magnitude in radio flux. The VLA+MERLIN results in HDF (Fig. 6) suggest that the radio sizes may be leveling off around $1''$ FWHM, but this may be due to the limited beam-size and point source sensitivity available in the deep radio surveys carried out thus far. One must be mindful that radio surveys at brighter levels produce exactly similar biases (Windhorst et al. 1984) The dotted line is the best power-law fit to all data below $S_{1.4} \simeq$10 Jy, which is arbitrarily extrapolated to $S_{1.4} \simeq$10 nanoJy.

The ratio of radio to optical–near-IR sizes of star-forming objects is close to unity at least at local redshifts (Deeg et al. 1997). While this may not be strictly true at very high redshifts, there is no a priori reason why the radio continuum (*i.e.*, synchrotron) emission should have been extended much further from the galaxy center than the optical–near-IR light, and therefore it is reasonable to assume that for faint star-forming objects the radio continuum sizes are to first order the same as the optical–near-IR sizes from the star-forming disk as seen by JWST. In Fig. 6, we plot therefore at the faint-end a box with the expected radio sizes (which should be considered an upper limit in their expected sizes), as estimated from the JWST discussion in §4 and Fig. 2–4. This box coincides with the power-law extrapolation (*cf.* Windhorst et al. 1993) of the radio sizes measured to 100μJy .

Fig. 6 then shows the natural confusion limit as expected for SKA. As in Fig. 2–4 for the optical–near-IR case, it was computed from the integrated radio source surface density, which was derived from the radio source counts in Fig. 5. Fig. 6 tentatively shows that the SKA will not run into the natural confusion limit at 100 nanoJy at 1.4 GHz. At levels of $S_{1.4} \simeq$10 nanoJy, the SKA will reach similar object surface densities as the JWST at J_{AB} $\simeq$33 mag (several to tens of 10^6 objects deg^{-2}). Like the JWST, the SKA may not run into the natural confusion limit at $S_{1.4} \simeq$10 nanoJy, *if* the slope of the nanoJy source counts remains below $\gamma \lesssim 1.7$ (i.e., a magnitude slope $\alpha \lesssim 0.28$), and *if* the radio continuum (NOT HI) and optical–near-IR sizes of star-forming objects remains similar at nanoJy levels, and continue to decline at fainter fluxes.

7. DISCUSSION AND CONCLUSION

The natural confusion limit in ultradeep surveys must be carefully addressed. The following are our conclusions, and future work will need to further study the following issues:

• **(1)** The JWST diffraction limit should be kept around 0.″08–0.″10 FWHM, and its optics should be kept as close to diffraction-limited as possible at the shortest wavelengths (0.6–2μm), to mitigate the effects from natural confusion in ultradeep surveys at the faintest flux levels ($J_{AB} \gtrsim$28–32 mag).

• **(2)** If most objects at $J_{AB} \gtrsim$26–28 mag are indeed largely unresolved at the 0.″08 FWHM of JWST, as our few simulations available in Fig. 4 thus far suggest, then SB-sensitivity is not the overriding factor in designing ultradeep surveys, but point source sensitivity and natural confusion will be. This sword cuts on two sides. If objects with at $J_{AB} \gtrsim$28–30 mag are largely unresolved, then their structure and morphology will be harder to measure with JWST. However, if indeed largely unresolved, they will not suffer the full cosmological $\propto(1+z)^4$ SB-dimming, but instead their bolometric fluxes will only dim as $\propto(1+z)^2$, which makes them easier to detect, even at very high redshifts in deep JWST surveys.

• **(3)** SKA will need 0.01–0.05″ FWHM or better to resolve the faintest starforming objects expected at large redshifts. These would be possibly objects of globular cluster-type mass or somewhat heavier that started shining around the epoch of reionization ($z_{ion} \simeq$6.5–7; Becker et al. 2001; Fig. 4 here). That is, to probe the epoch of reionization, SKA will need trans-continental sized baselines at 1.4 GHz (800-4000 km). Dynamic range and point-source sensitivity is critical for the SKA, but SB-sensitivity at scales$\gtrsim$0.3″ may not be as important for faint continuum objects at least. SKA will then be able to measure sizes for very small objects ($r_e \simeq$0.″01), which would require a D$\gtrsim$60 meter telescope in space at near-IR wavelengths. However, at nanoJy levels, JWST will likely detect such objects as point sources well before SKA can detect and resolve them at $S_{1.4} \simeq$10 nJy.

For both radio and optical–near-IR surveys at nanoJy levels, we conclude that, counter to expectations, surface-brightness sensitivity may not be as important as the best possible resolution and point-source sensitivity for FWHM$\simeq$0.″08. The caveat here, of course, is that for larger objects at more intermediate redshifts (z$\sim$1–4 or $r_e \lesssim$0.″5–1.″0), SB-sensitivity is of utmost importance, so that telescopes like the SKA will have to be designed to have both excellent point-source sensitivity (at $\lesssim$0.″1 FWHM resolution) and excellent SB-sensitivity (at 0.″5–1.″0 FWHM). This is especially true because the fully two-dimensional spectroscopic capability of these future telescopes (i.e., redshifted H-I mapping for SKA and the Micro Shutter Array (MSA) slit-lets in NIRSpec for JWST) will allow us to some extent spectrally disentangle objects at $A_B \gtrsim$30 mag, even if they did

spatially significantly overlap.

• **(4)** To better deal with the natural confusion limit, a new generation of object finding and parameter determining algorithms may be needed that takes into account what is known about the instrumental PSF and the pix-to-pixel statistics of the image-noise, and makes best fits to each detected object while trying to optimally de-blend it from its neighbors. These algorithms may need to be updated to include *simultaneous* object fitting techniques such as currently used in crowded star-fields. Additional information that can help here is the photo-z information for each fitted sub-clump of a cluster of objects, and with the arrival of SKA also redshifted HI information in the high-resolution data cubes that include the redshifted HI-line flux.

• **(5)** Better predictions about the expected nature of the faint object population and its role in the natural confusion limit will also come from larger and higher resolution full-numerical and/or semi-analytical models. These together can help us predict the size distribution of objects at AB$\simeq$28–36 mag, which will be of utmost importance when designing these ultradeep optical-IR—radio surveys of the future.

We thank David Burstein, Ron Ekers, Ray Norris, Lister Staveley-Smith and Pete Stockman for helpful discussions. We thank the ATNF staff for their hospitality during a working visit, where part of this work was done. RAW, RAJ, SHC and SCO acknowledge funding for the HST part of this study from National Aeronautics and Space Administration (NASA) grants GO.5985.01.94A, GO.6609.01.95A, AR.7534.02.96A and AR-8357.01 by the Space Telescope Science Institute (STScI). AMH acknowledges support provided by NASA through Hubble Fellowship grant HF.01140.01-A awarded by STScI. STScI is operated by the Association of Universities for Research in Astronomy, Inc., under NASA contract NAS5-26555. We also acknowledge funding for the JWST part of this study from NASA Grant NAG5-12460. R. Windhorst thanks the AAS for a travel grant to the ATNF that made the start of this project possible. S. Cohen would like to thank the ASU NASA Space Grant Graduate Fellowship.

We acknowledge the Astronomical Data Analysis Center of the National Astronomical Observatory, Japan, where the numerical computations for this paper were performed. BKG and DK also acknowledge the Australian Research Council.

REFERENCES

Abraham, R. G., Tanvir, N.R., Santiago, B.X, Ellis, R.S., Glazebrook, K., van den Bergh, S. 1996, MNRAS, 279, L47

Becker, R. H., et al. 2001, AJ, 122, 2850

Benn, C. R., Grueff, G., Vigotti, M., & Wall J. V. 1982, MNRAS, 200, 747

Bertin, E., & Arnouts, S. 1996, AJ, 117, 393

Bertschinger, E. 2002, ApJS, , 137, 1

Bruzual A., G. & Charlot, S. 1993, ApJ, 405, 538

Burstein, D., Haynes, M. P., Faber, M. 1991, *Nature*, 353 515

Carlberg, R. G. 2002, ApJ, 573, 60

Cohen, S. H., Windhorst, R. A., Chiarenza, C. A. T., Odewahn, S. C., & Driver, S. P. 2002, AJ, submitted

Condon, J. J. 1974, ApJ, 188, 279

Deeg, H.-J., Duric, N., Brinks, E. 1997, A&A, 323, 323

Driver, S. P., et al. 1998, ApJL, 496, L093 (astro-ph/9802092)

Driver, S. P., Windhorst, R. A., Ostrander, E. J., Keel, W. C., Griffiths, R. E., & Ratnatunga, K. U. 1995a, ApJL, 449, L023

Ekers, R. D. 2000, in "Looking Deep in the Southern Sky", Proceedings of the ESO/Australia Workshop, p. 146, Eds. F. Morganti and W. J. Couch (Berlin: Springer-Verlag)

Ellis, R. S. 1997, ARA&A, 35, 389 (astro-ph/9704019)

Fomalont, E. B., Partridge, R. B., Lowenthal, J. D., & Windhorst, R. A. 1993, ApJ, 404, 8

Fomalont, E. B., et al. 2002, AJ, 123, 2402 (astro-ph/0201441)

Gardner, J. P., & Satyapal, S. 2000, AJ, 119, 2589

Gardner, J. P. 1998, PASP, 110, 291

Gibson, B.K., Fenner, Y., Renda, A., Kawata, D., & Lee, H.-C. 2003, PASA, 20, 401

Glazebrook, K., Ellis, R. E. Santiago, B. & Griffiths, R. E. 1995b, MNRAS, 275, L19

Haiman, Z., & Loeb, A. 1998, ApJ, 519, 479

Hammer, F., Crampton, D., Lilly, S., LeFevre, O., Kenet, T. 1995, MNRAS, 276, 1085

Hogg, D. W. 2001, AJ, 121, 1207

Hopkins, A., Windhorst, R. A., Cram, L., & Ekers, R. 2000, Experimental Astronomy, Vol. 10, No. 4, 419 (astro-ph/9906469).

Hopkins, A., Afonso, J., Cram, L., Mobasher, B. 1999, ApJ, 519, L59

Im, M., & Stockman, H. S. 1999, in "Astrophysics with Infrared Surveys: A Prelude to SIRTF", ASP Conference Series, Vol. 177, p.75 Eds. Ed. M. D. Bicay, R. M. Cutri, and B. F. Madore. See also http://www.stsci.edu/ngst/science/simulations/im/

Kawata, D. 2001, ApJ, 548, 703

Kawata, D., & Gibson, B.K. 2003a, MNRAS, , 340, 908

Kawata, D., & Gibson, B.K. 2003b, MNRAS, , 346, 135

Kodama, T., & Arimoto, N. 1997, A&A, 320, 41

Koo, D. C., & Kron, R. G. 1992, ARA&A, 30, 613

Kron, R. G., Koo, D. C., & Windhorst, R. A. 1985, A&A, 146, 38

Liske, J. et al. 2002, MNRAS, (astro-ph/0207555)

Maihara, T. et al. 2001, PASJ, 53, 25

Marzke, R. O., Da Costa, L. N., Pellegrini, P. S., Willmer, C. N. A. & Geller, M. J. 1998, AJ, 503, 617

Mather, J. C., Stockman, H. S. 2000, Proc. SPIE Vol. 4013, p. 2-16, in "UV, Optical, and IR Space Telescopes and Instruments", Eds. J. B. Breckinridge & P. Jakobsen (Berlin: Springer)

Odewahn, S. C., Windhorst, R. A., Driver, S. P., & Keel, W. C. 1996, ApJL, 472, L013

Odewahn, S. C., Cohen, S. H., Windhorst, R. A., & Philip, N. S. 2002, ApJ, 568, 539 (astro-ph/0110275)

Petro, L. 2001, the Next Generation Space Telescope Simulator NMS, STScI, www.ngst.stsci.edu/nms/main/nms_flux_form.html

Richards, E. A. 2000, ApJ, 533, 611

Rieke, M. et al. 2002, Proc. SPIE Vol. xxxx, in press in "AstronomicalTelescopes and Instrumentation", Eds. R. Angel and J. B. Breckinridge (Berlin: Springer). See also http://ircamera.as.arizona.edu/nircam/

Scheuer, P. A. G. 1974, MNRAS, 166, 329

Stockman, H. S., Mather, J. C. 2000, in "The Extragalactic Infrared Background and its Cosmological Implications", IAU Symp. No. 204, p. 37 (Dordrecht: Kluwer)

Tyson, J. A. 1988, AJ, 96, 1

Windhorst, R. A., et al. B., Richards, E., Franklin, B. E., Pascarelle, S. M., & Griffiths, R. E. 1995, *Nature*, 375, 471

Windhorst, R. A., Fomalont, E. B., Partridge, R. B., & Lowenthal, J. D. 1993, ApJ, 405, 498

Windhorst, R. A., Miley, G. K., Owen, F. N., Kron, R. G., & Koo, D. C. 1985, ApJ, 289, 494

Windhorst, R. A., et al. 2000, in "The Hy-Redshift Universe: Galaxy Formation and Evolution at High Redshift", Eds. A. J. Bunker & W. J. M. van Breugel, ASP Conf. Ser. Vol. 193 (Provo, UT: Brigham Young University), p. 55

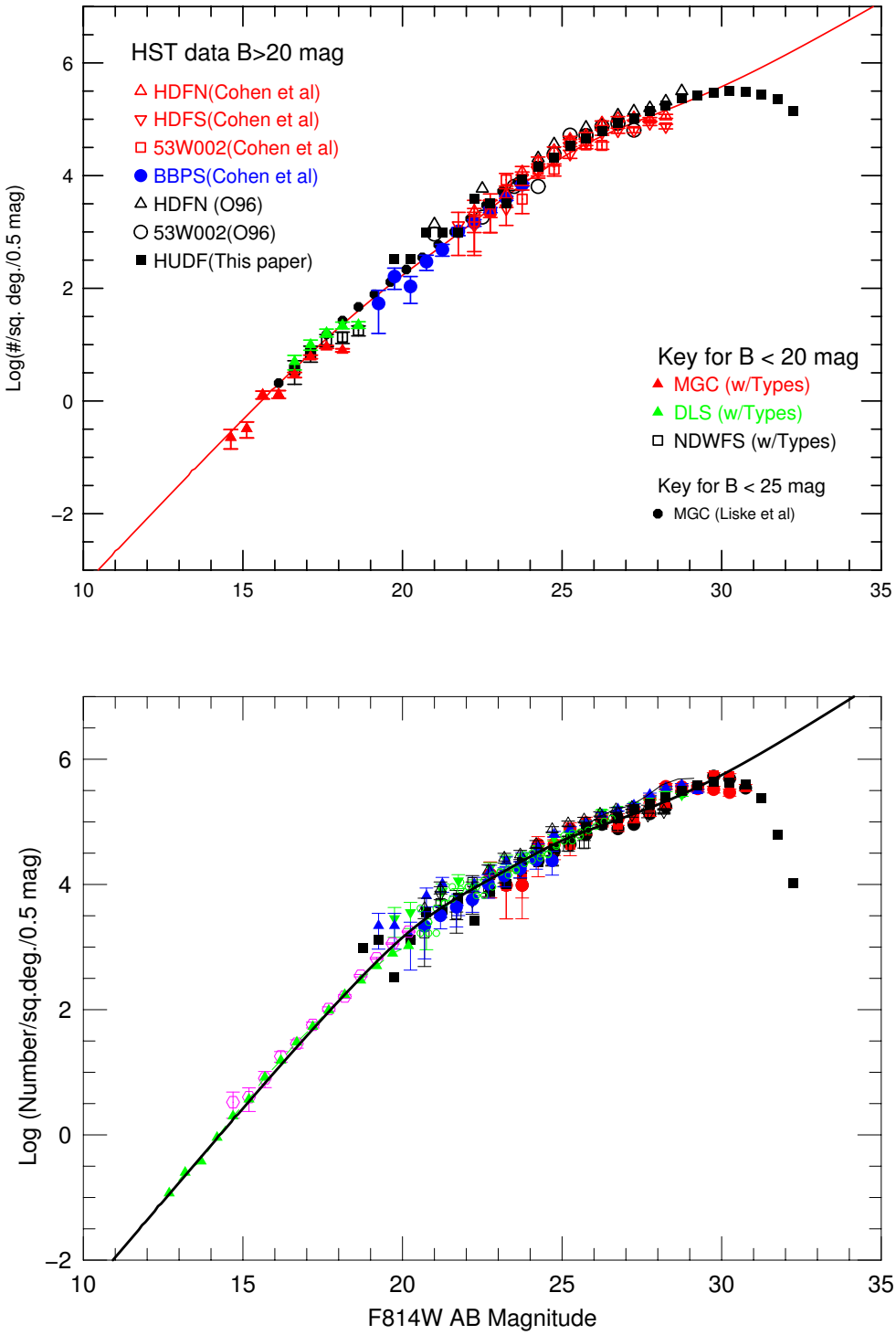

Fig. 1.— Fig. 1. B-band counts and I-band counts including the HST UDF counts. Individual surveys are discussed in Cohen et al. (2003, 2004). Models are from Cohen et al. (2003) and Gardner & Satyapal (2000), who modeled the observed number counts to A_B =29 mag using luminosity and SED evolution of the stellar populations and number density evolution due to reasonable merger scenarios. Gardner & Satyapal (2000) also extrapolated these model counts to longer wavelengths (J_{AB}). At $\lambda \gtrsim 1\mu$m, the surface density at A_B =34 can exceed 10^7 objects deg^{-2} , depending on the exact model used, which is an important consideration for the calculation of the natural confusion limit (see Fig. 2–4).

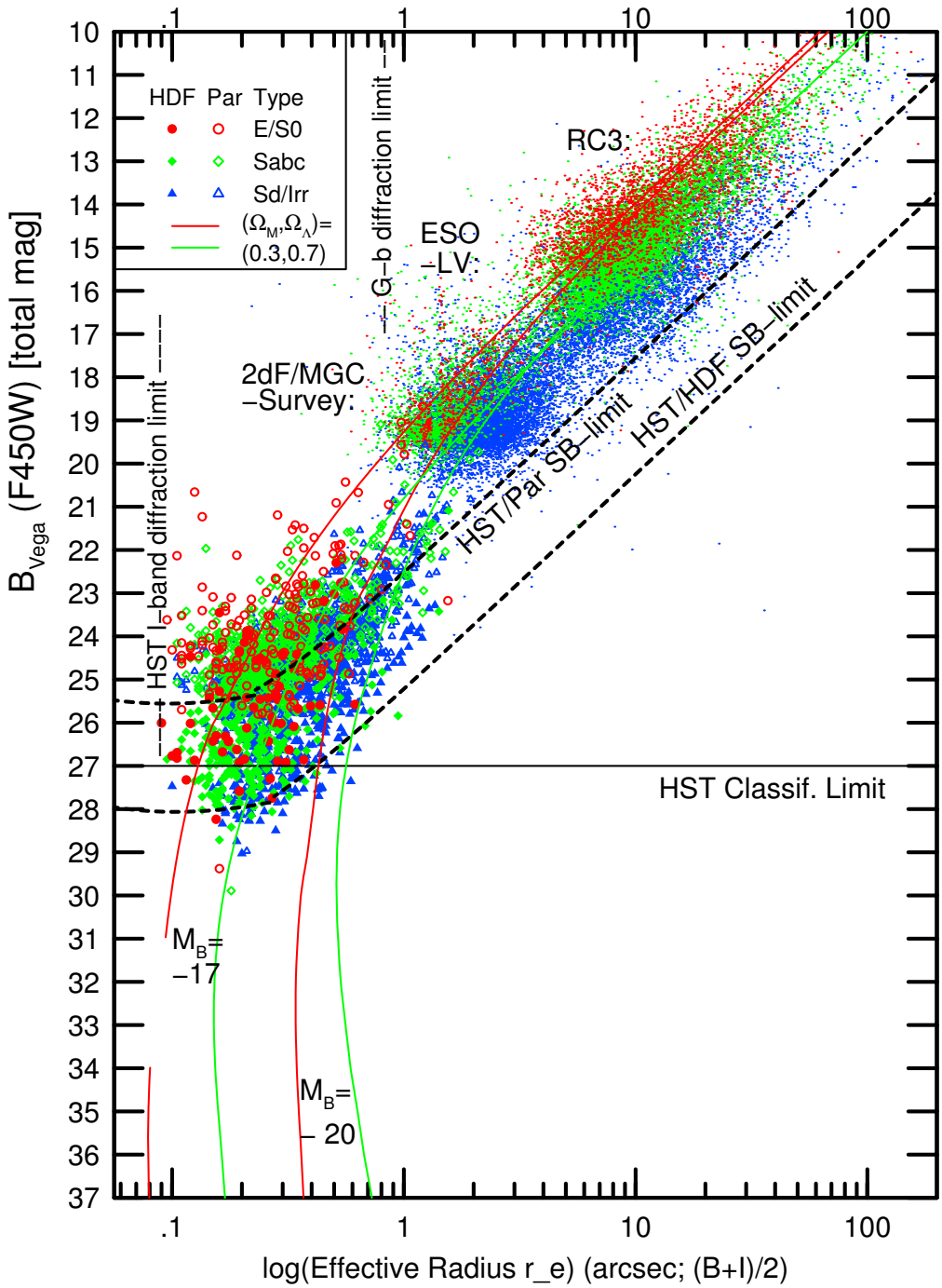

Fig. 2.— Fig. 2. Summary of the relation between B–band flux (B_J -mag) and effective or half-light radius (r_e) for the entire galaxy population from the RC3 level to the HDF limit ($B_J \simeq$10–28 mag). Plotted are the ground-based RC3 and ESO Lauberts-Valentijn samples, which are both photographic surveys, but with good r_e measurements and galaxy types available, as well as the 2dF/MGC survey (Liske et al. 2002), which is a wide-area CCD survey with the 2.5 m INT telescope. At the faint end, the HST Parallel surveys are plotted, as well as three deep HST surveys including the two HDF's (Cohen et al. 2002, Odewahn et al. 1996). All fluxes are on the Vega B_J system (e.g., Kron 1980), since this is the only system currently publicly available with consistent data in the entire flux range $A_B \simeq$10–28 mag. Symbols are color-coded according to ANN galaxy-type, as the legend indicates. The black dashed lines represent the point-source and SB-detection limits for Parallel and deep HST surveys, modeled through an exponential disk convolved with a Gaussian PSF (Cohen et al. 2002). *Note that the HDF data does not straddle the HST SB-limit well around $r_e \simeq 1''$, which may be due to the onset of the natural confusion limit (see Fig. 4).* The red and green curves that are almost vertical at the faint end give the B_J –r_e relations predicted from the type-dependent median sizes observed in the RC3 (which have median $M_B \simeq$–20 mag), redshifted for the cosmology in the legend. The black horizontal line at $B_J \simeq$27 mag indicates the HST classification limit. The $M_B =$–20 mag models show that most faint galaxies (of all types) are smaller than the median RC3 sizes, indicating the lower galaxy luminosities sampled at fainter fluxes, and suggesting the hierarchical growth of galaxy sizes with time.

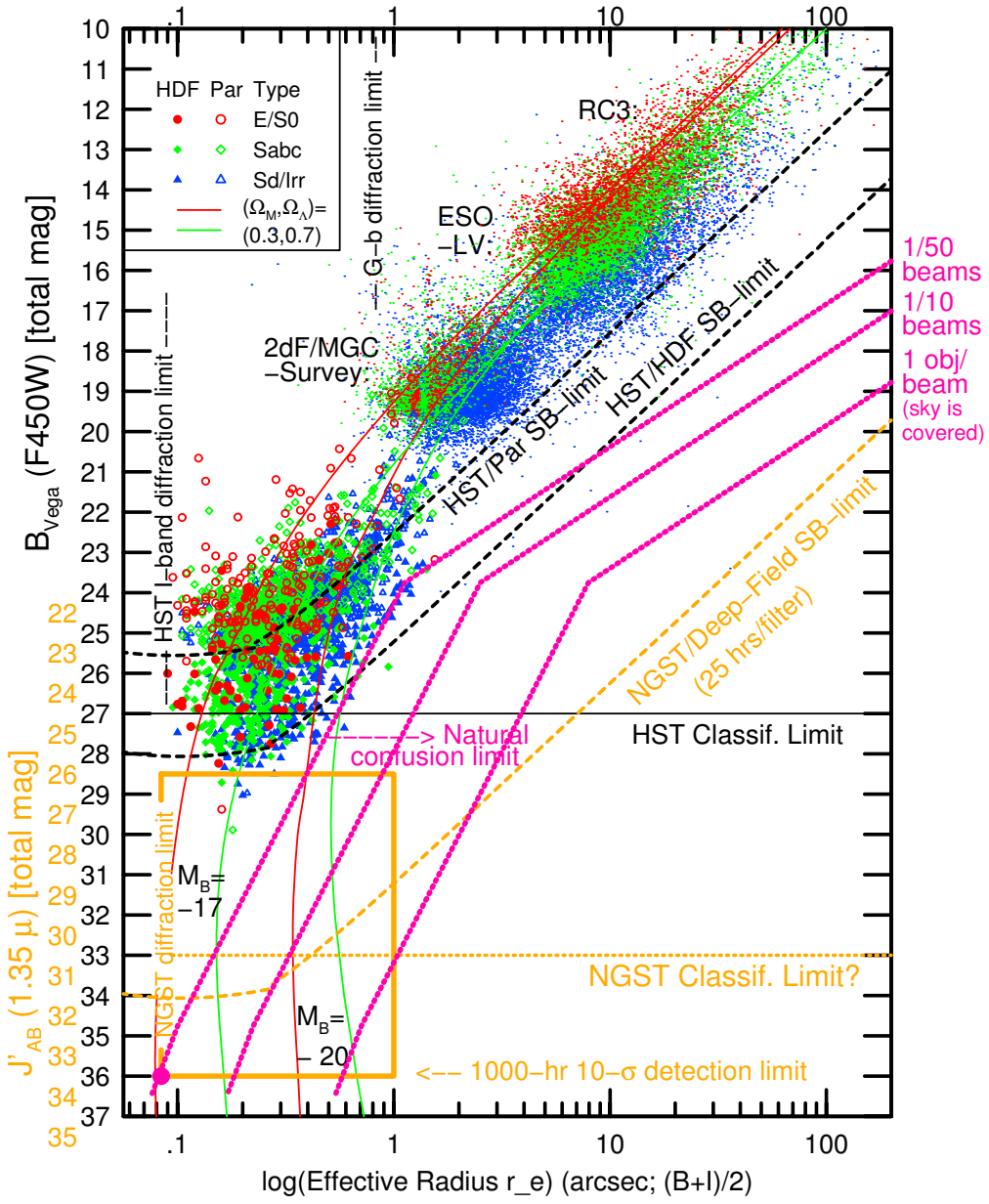

Fig. 3.— Fig. 3. Same as in Fig. 2, but with the JWST sensitivity limits also plotted in orange, and with the natural confusion limits plotted in pink. For $B_J \gtrsim 28$ mag we adopt a J_{AB} flux scale, since JWST is not sensitive in the B_J -filter or anywhere below 0.6μm, and since the median redshift is expected to be $z_{med} \gtrsim 1$–2 (Driver et al. (1998) with a significant tail at z$\gtrsim$ 4, causing B-band drop-outs. For reasonable redshift distributions at $A_B \gtrsim 28$ mag ($z_{med} \simeq$2–4 and with a tail to $z_{max} \simeq z_{ion} \simeq$7–10), J_{AB} -mags transform approximately to B_J -mag as indicated by the orange scale to the left. The J_{AB} point-source and SB-limit for a 25-hr JWST exposure are indicated by the curved orange dashed lines, and was computed as for the HST surveys in Fig. 2. The expected JWST classification limit is similarly indicated, although it is likely uncertain. Also indicated is the 10-σ J_{AB} point-source sensitivity limit for a 1000-hr "super-HDF-like" JWST campaign. The natural confusion limits are indicated by the three pink lines, which follow from *integrating* the I_{AB} galaxy counts in Fig. 1b (Gardner & Satyapal 2000), converted to J_{AB} using a Bruzual & Charlot (1993) model. The natural confusion lines are drawn for the level of 50 independent "beams" (or $\pi r_e{}^2$'s) per detected object (i.e., the classical confusion limit, but now due to finite object sizes); at 10 independent "beams" per detected object; and at 1 "beam" per detected object, which is the level where the sky would be covered with half-light radii and started to look like a globular cluster. *Note that the HDF data does not straddle the HST SB-limit well around $r_e \simeq 1''$, which may indeed be due to natural confusion setting in around $B_J \simeq 24$ mag. This, however, would have only caused a relatively small fraction of the galaxies in the HDF being missed for $B_J \simeq 24$–28 mag by the SExtractor algorithm — see the discussion of blended objects by Williams et al. 1996).* The triangle bounded by the JWST diffraction limit (vertical orange line) and the slanted pink line for the 1/50 natural confusion limit is where most JWST objects are expected. Following the plotted models, these would have $M_B = -17$ mag or fainter. If all these faint JWST objects straddled the pink line, the deep JWST samples would be limited by natural confusion. However, we will argue in Fig. 4 that objects with $J_{AB} \gtrsim 28$ mag are likely mostly unresolved, and so they will instead straddle the JWST diffraction limit and skirt away from the 1/50 natural confusion limit line.

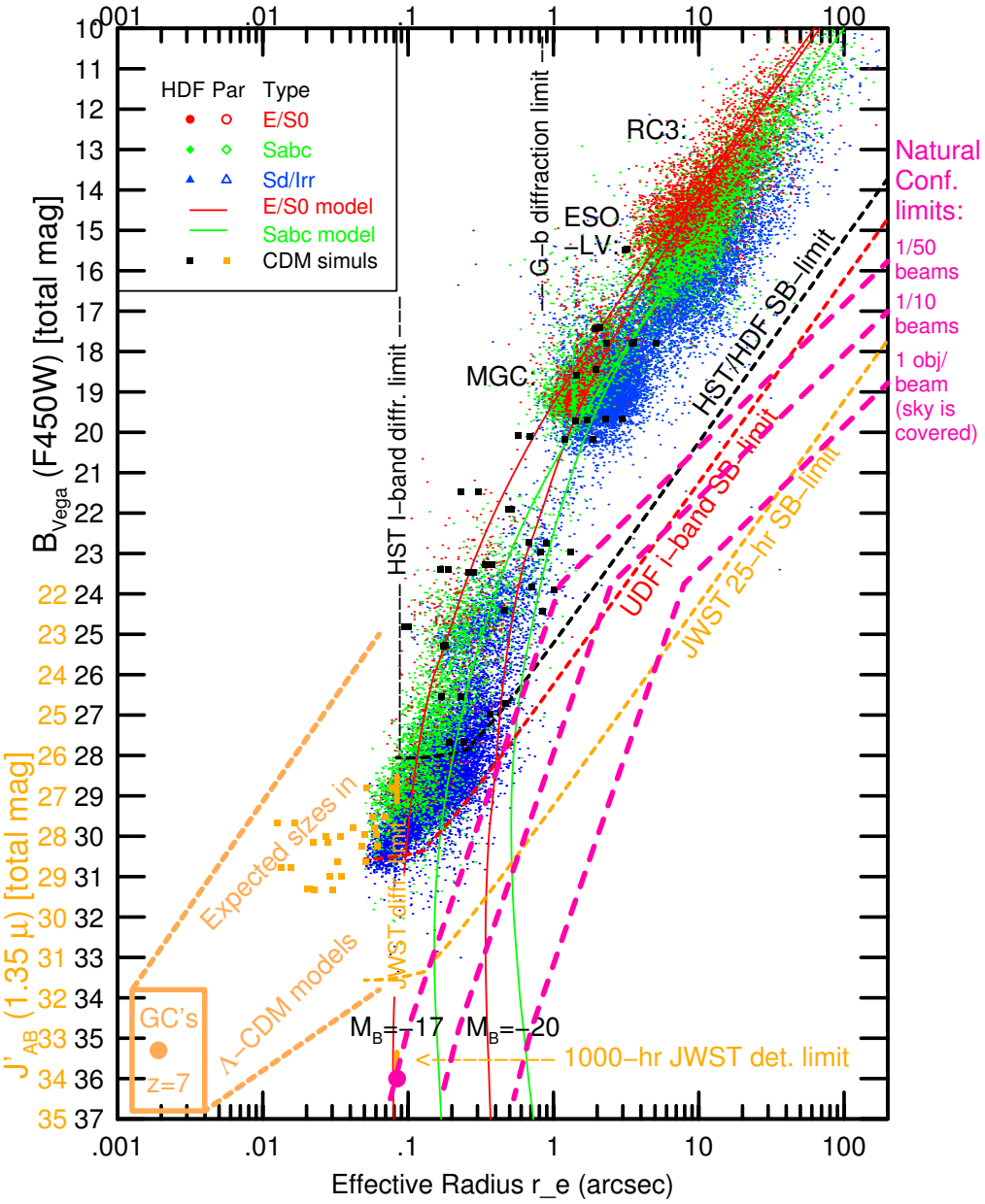

Fig. 4.— Fig. 4. Same as in Fig. 2–3, but with the 1000-hr JWST point-source and SB-sensitivity limits also plotted in orange, and the same natural confusion limits as in Fig. 3 in pink. The general area to the lower-right of the 1/50 and 1/10 natural confusion lines is not surveyable with sample completeness and reliability better than 98% and 90%, respectively, because of object overlap. Our available ΛCDM numerical simulations using the models of Kawata (2001a, 200b) are plotted for $B_J \lesssim 28$ mag as black filled squares (using the B_J -mag scale, since most of these have simulated $z \lesssim 4$). The good agreement between the black simulated galaxies and the observed colored points in the HDF for $B_J \lesssim 28$ mag gives us confidence that the few available simulations for $J_{AB} \gtrsim 26$ may yield accurate galaxy sizes. Also shown is the expected size-range and flux-range for objects of globular cluster-type mass around the epoch of reionization ($z \simeq 7$). The expected object sizes in ΛCDM cosmological simulations for $J_{AB} \gtrsim 26$–28 mag fall mostly below the JWST diffraction limit ($\simeq 0''.08$ FWHM). If this is indeed true, then the deepest JWST images will be limited by the *instrumental* confusion limit (as determined by JWST's instrumental FWHM$\simeq 0''.08$), which doesn't set in until $J_{AB} \gtrsim 33.5$ mag (big pink dot). In that case, the hierarchical formation of galaxies together with the effects of the cosmological constant Λ at $z \lesssim 0.8$ (Cohen et al. 2002) conspire to just keep the deepest JWST surveys away from the natural confusion limit (pink lines). We plan on doing more ΛCDM numerical simulations of galaxy sizes with $J_{AB} \simeq 26$–34 mag and $r_e \simeq 0''.001$–$0''.2$ to confirm these findings. *Our most important conclusion is that deep JWST surveys for $J_{AB} \gtrsim 26$ mag, and even deep HST surveys for $B_J \gtrsim 24$ mag, start to become more limited by natural confusion than by the traditional SB-limitations. Yet, both are mostly limited by the point-source sensitivity of these telescopes. These findings must be further investigated by studying the behavior of object-finding algorithms on simulated images, as this issue will likely directly impact the technical specifications of future telescopes (e.g., the FWHM and the exact PSF-shape of the JWST and SKA), and the nature of future ultradeep surveys at nanoJansky levels. The 150-orbit ACS i-band limits are also shown, and helps address the natural confusion limit for JWST.*

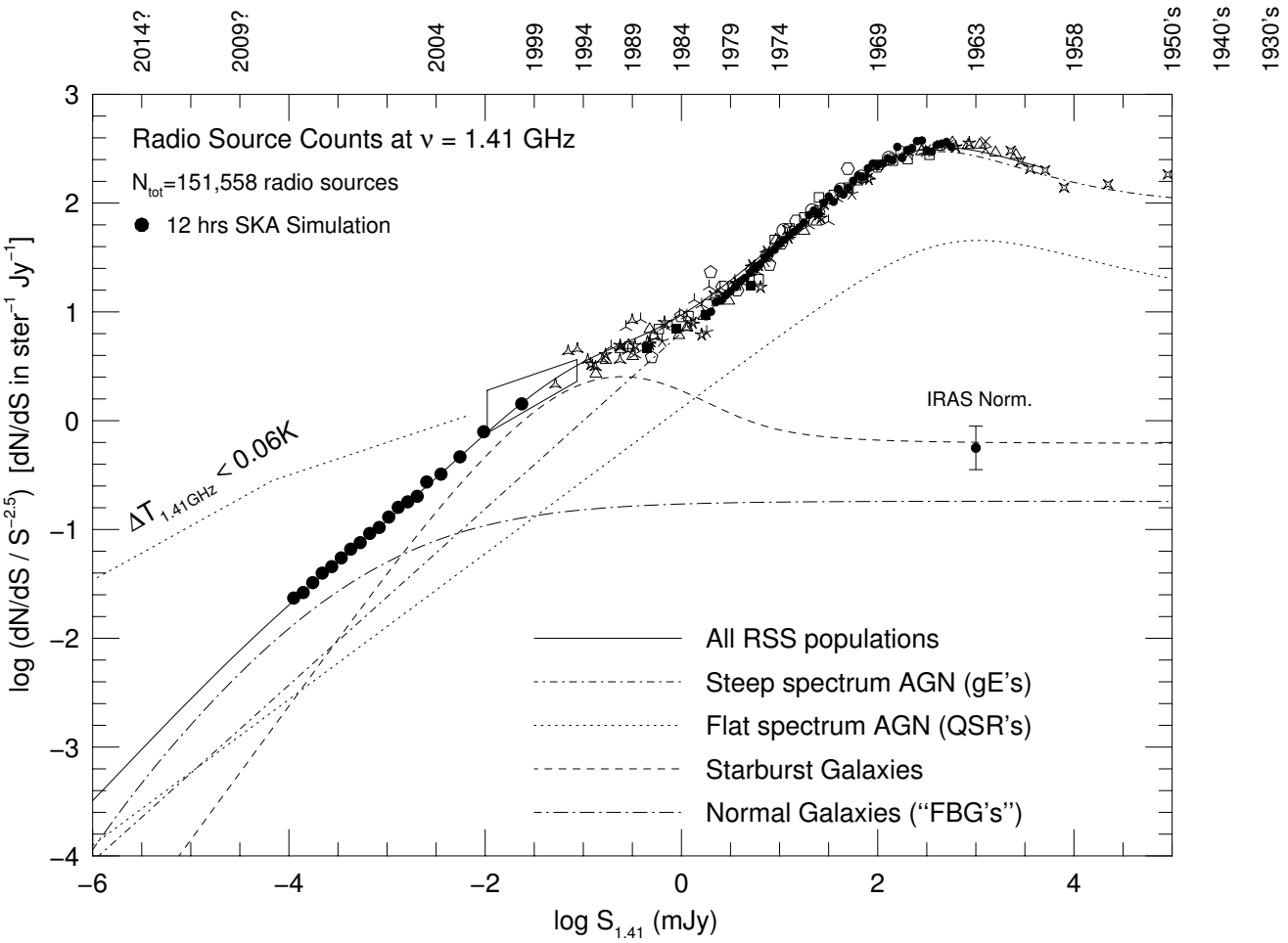

Fig. 5.— Fig. 5. The observed normalized differential 1.41 GHz source counts. The various symbols are existing observed source counts, taken from surveys reviewed in Windhorst et al. (1993, 1999). Filled circles between 100 nJy–10μJy indicate a 12-hr simulation with the Square Kilometer Array (Hopkins et al. 2000). The straight dotted lines represents the upper limit to the nanoJy source counts from CBR temperature constraints (Fomalont et al. 1993, Windhorst et al. 1993). Models of the source counts are from Hopkins et al. (2000) as follows: Dashed line: IRAS-type population; Dotted line: AGN flat-spectrum population ("Quasars"); Dot-dashed line: AGN steep-spectrum population ("Giant elliptical galaxies"); Dot-dash-dotted line: normal galaxy population; Solid line: sum of all populations. The maximum possible contribution is shown for the normal galaxy population (dot–long-dash). The extrapolation of the 1.4 GHz source counts below 10μJy is uncertain by at least 0.3 dex in the range 10–100 nJy (see Hopkins et al. 2000), depending on whether the high IRAS normalization is used for normal spirals, the standard normalization (as plotted here), or no normal spirals are added altogether.

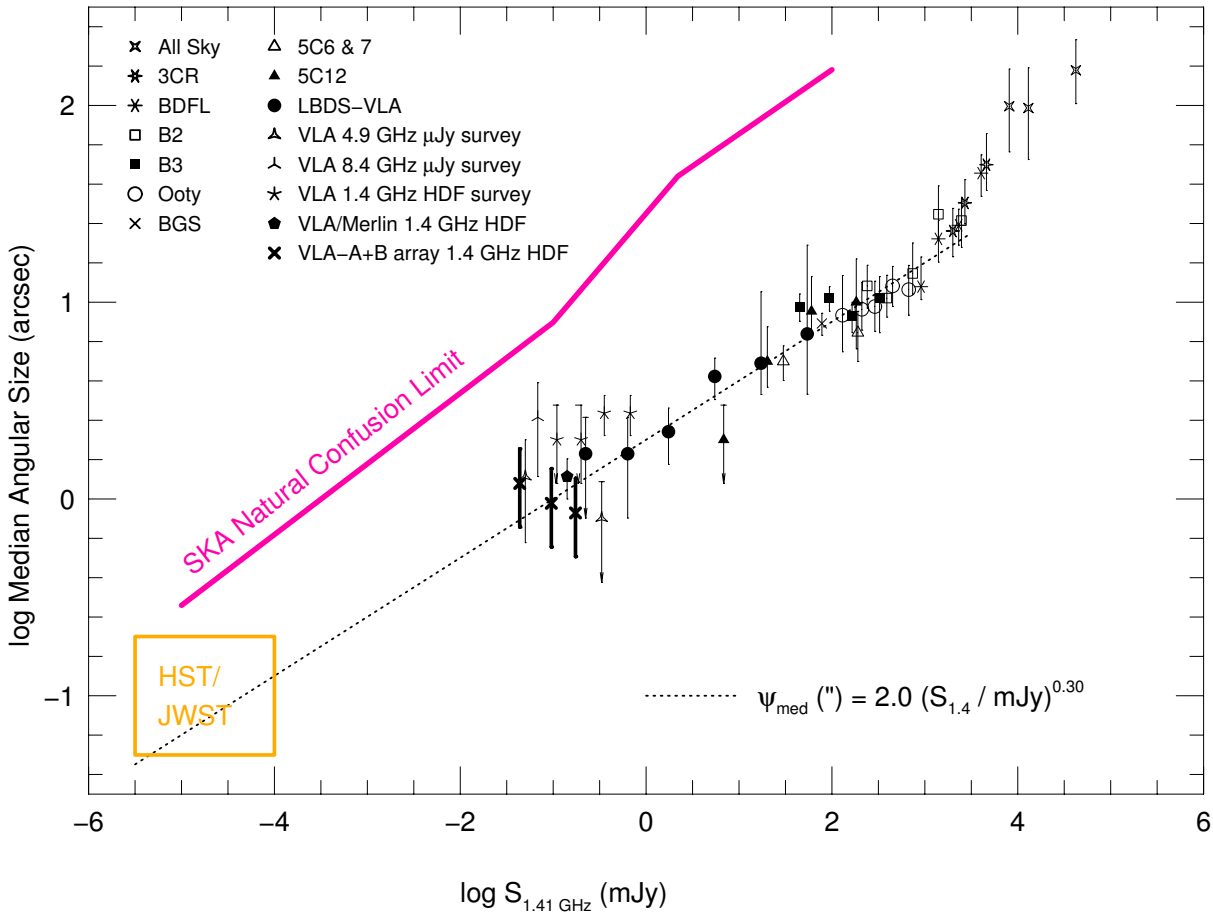

Fig. 6.— Fig. 6. Median angular size vs. 1.41 GHz flux for low-frequency surveys, and for the deepest VLA surveys at 8.4, 4.86 and 1.4 GHz (Windhorst et al. 1993, Richards 1999, Fomalont et al. 2002). All flux scales were transformed to 1.41 GHz following the α_{med} vs S_ν relation of Windhorst et al. (2000). The dotted straight line is the best fit for $0.1 \lesssim S_{1.4} \lesssim 3000$ mJy, and was arbitrarily extrapolated as a straight power-law to 10 nanoJy. This extrapolation meets with the median JWST sizes expected at nanoJy levels, where both the extrapolated 1.4 GHz radio counts and the JWST object counts reach surface densities of several to tens of million per deg^2 . This suggests, although does not prove, that the expected SKA source sizes at 10–100 nanoJy may be $<<0''.1$. Hence, if the faintest radio emitting objects seen by SKA are also dominated by faint hierarchical growing objects as expected for JWST (Fig. 2–4), then the SKA will likely also remain below the natural confusion limit, provided that its longest baselines are several 1000 km at 1.4 GHz, so that its resolution is (much) better than $0''.05$ FWHM (see Fig. 2–4).